INTERNATIONAL JOURNAL FOR NUMERICAL METHODS IN FLUIDS
Int. J. Numer. Meth. Fluids 2009; **61**:796–809
Published online 22 December 2008 in Wiley InterScience (www.interscience.wiley.com). DOI: 10.1002/fld.1985

Numerical simulation of tangentially injected turbulent swirling flow in a divergent tube

Hui-Fen Guo[1] and Zhi-Yong Chen[2,*,†]

[1]*Textile College, Donghua University, Shanghai 201620, People's Republic of China*
[2]*Shanghai Institute of Applied Mathematics and Mechanics, Shanghai University, Shanghai 200072, People's Republic of China*

SUMMARY

This paper studies the properties of turbulent swirling decaying flow induced by tangential inlets in a divergent pipe using the realizable k–ε turbulence model and discusses the effects of the injector pressure and injection position. The results of transient solutions show that both the recirculation zone near the wall in upstream of the injectors and the vortex breakdown in downstream of the injectors increase in size during the whole period. A nearly axisymmetric conical breakdown is formed and its internal structure consists of two asymmetric spiral-like vortices rotating in opposite directions. The stagnation point shifts slowly toward the pipe outlet over time. The maxima of the three velocity components, which are located near the wall, decrease gradually with streamwise direction. It can also be inferred that Mach number approaches 1.0 near the injector outlets. The velocities increase with the increasing injector pressure. However, its increasing trend is not significant. With the increase of the injection position, vortex breakdown moves in downstream direction and the pitch along the streamwise direction increases. Copyright © 2008 John Wiley & Sons, Ltd.

Received 5 July 2008; Revised 7 November 2008; Accepted 11 November 2008

KEY WORDS: swirling flow; vortex breakdown; recirculation zone; tangential inlets; injector; diverging pipe

1. INTRODUCTION

Swirling flow has been applied in a wide range of engineering devices, such as cyclones, separators, combustions, gas turbines, etc. In the 1960s, turbulent swirling decaying flow was applied to produce air-jet spun yarn. Owing to advantages in processing speed and cost, air-jet spinning is

*Correspondence to: Zhi-Yong Chen, Shanghai Institute of Applied Mathematics and Mechanics, Shanghai University, Shanghai 200072, People's Republic of China.
†E-mail: chenzychina@126.com

Contract/grant sponsor: Key Basic Research Foundation of Shanghai; contract/grant number: 08JC1400300

accepted as one of the most promising technologies. For prevailing Murata jet spinning system, the forming yarn is 'twisted' by operating two swirling air currents in mutually opposite directions in two nozzles. At present, most of the information available in the literature on air-jet spinning, which was based on spinning experiments, was related to the yarn structure [1–3], the principle of yarn formation [1, 4] and the effects of various parameters on yarn quality [1–3, 5]. All these mainly depend on the fiber motion, which is closely related to the flow characteristics, so it is important to study the airflow in the nozzles. However, little work has been reported regarding flow characteristics in the two nozzles of the air-jet spinning, especially in the second nozzle.

According to the different functions of two nozzles in air-jet spinning, normally the first and second nozzles are made cylindrical and diverged conical shapes, respectively. The flow field in the first nozzle has been experimentally and numerically studied in our research team. Owing to the limitation of experimental conditions, Yu and Zhang [6] used LDV to measure only the velocities at the injector and nozzle outlets under the Reynolds similarity. Zeng and Yu [7] used numerical method to study two-dimensional steady airflow characteristics in the first nozzle and discussed the effects of the nozzle design parameters (injection angle and injector position) on yarn properties. However, their predictions [6, 7] cannot show certain properties of the swirling flow since the flow instabilities are three-dimensional and time dependent in nature [8]. In order to investigate more deeply the flow field in the first nozzle (including the slotting-tube), three-dimensional flow characteristics have been studied by Guo *et al.* [9–12]. The flow patterns show clearly periodic change and the velocity appears to be decaying over time. Spiral vortex breakdown is also observed in the downstream of the injectors, and its occurrence migrates downstream toward the nozzle outlet as time is increased. It is obvious that the flow behavior in the second nozzle (a diverging tube) is different from that in the first nozzle (straight circular pipe). To the authors' knowledge, few publications have reported regarding the flow field in the second nozzle. Only earlier report [9] studied the steady flow characteristics in the second nozzle with a small injector diameter. Hence, the present work is dedicated to a numerical analysis of three-dimensional transient swirling flow in the second nozzle of air-jet spinning.

In air-jet spinning, the swirling flow in the nozzle is produced by tangentially injecting high-velocity compressed air into a tube through evenly spaced injectors. Studies of the swirling flow in a divergent pipe are, however, rather scarce. The effect of changing the cross-sectional area of a pipe on a stream of rotating fluid was first studied in the work of Batchelor [13]. He noticed that the family of solutions describes two possible equilibrium states as swirl is increased for inviscid swirling flows in a diverging pipe. Batchelor's work has motivated a recent theoretical study by Buntine and Saffman [14], who examined the development of inviscid, steady swirling flows in a finite-length diverging pipe. They claimed that when a stagnation point appeared along the pipe outlet, non-regular solutions that should describe a separation zone must develop. The flow inside the separation zone cannot be determined solely by the inlet conditions. Rusak *et al.* [15] investigated the effect of small pipe divergence on an inviscid, incompressible, near critical axisymmetric swirling flow. They demonstrated the singular behavior of solutions of the Euler equations around the critical swirl. Pipe divergence creates an adverse pressure gradient that promotes the development of large disturbance waves at swirl levels that are less than the critical swirl. Sarpkaya [16] and Sarpkaya and Novak [17] presented experimental results for vortex breakdown in a diverging pipe (water was used as test fluid), and considered the resulting 'conical' breakdown fundamentally distinct from the various forms of laminar breakdown. Recently, Spall and Ashby [18] simulated turbulent vortex breakdown within a slightly diverging tube for the incompressible fluid. The results showed that the standard k–ε model failed to predict the occurrence

DOI: 10.1002/fld

of breakdown. However, the differential Reynolds stress model (RSM) predicted satisfactorily the mean azimuthal and axial velocity profiles downstream of the breakdown.

For the numerical prediction of swirling flow properties in engineering practice RANS-type turbulence models are state of the art. Many studies have shown that the standard k–ε two-equation turbulence model (KEM) in general performs poorly due to the neglect of both anisotropic viscosity and additional turbulence generation arising from the effects of streamline curvature [18, 19]. In the literature, several modifications of the standard KEM have been proposed for swirling flows. For example, Khodadadi and Vlachos [20] have proposed to use different values of the model constants. However, the proposed values are not generally applicable. Among others, Chang and Chen [21], Kim and Chung [22] and Sloan *et al.* [23] have proposed to take into account the enhanced turbulence diffusion caused by the extra strain rate incorporated with streamline curvature to modify the standard KEM. However, none of the existing modified KEMs were reported to be able to yield satisfactory predictions of swirling flows with the swirl intensities ranging from low to high extents. For example, Sloan *et al.* [23] found that the modified KEM was inadequate for predictions of the toroidal recirculation zone (CTRZ).

Higher-order turbulence closure models such as the algebraic stress models (ASM) and RSM were also employed to improve computational accuracy. Weber *et al.* [24] tested three turbulence models in a simulation of confined turbulent swirling flows: a KEM, a RSM and an ASM. It was shown that RSM and ASM perform better than the KEM. However, Fu *et al.* [25] also pointed out that the ASM hypothesis seriously misrepresented the diffusive transport of the stress components and this defeat was aggravated by a failure accounting for additive swirl-related stress transport terms in the algebraic modeling process. Nagendra [26] has shown that RSM predicts worse the mean flow properties and best the turbulence kinetic energy. Hence, it is not clear whether the high-order models are more valuable than the KEM. In the last few years, both large eddy simulation (LES) and direct numerical simulation (DNS) have been used by several authors to predict swirling flows [27–29]. They have confirmed that the computational results are qualitatively in good agreement with the experimental ones. However, LES and DNS are still time consuming and immoderate for most engineering flow applications.

Despite the advances in modeling turbulent flow, the KEMs still remain commonly used model in the prediction of turbulent swirling flow. Recently, Shih *et al.* [30] proposed a realizable KEM, which consists of a new model dissipation rate equation and a new realizable eddy viscosity formulation. It has shown substantial improvements on the standard KEM where the flow features include strong streamline curvature, vortices and recirculation. Nagendra [26] applied the realizable KEM to confined swirling recirculating jet, and found that it has been good in predicting the mean flow, especially in the downstream region and in the near axis region. Hence, based on engineering application and economy of computer efforts, the realizable KEM is adopted to simulate 3-D swirling flow characteristics in the diverging tube. Since the injector pressure and injection position are the two most important parameters in air-jet spinning, their effects on fluid flow are also discussed.

2. GOVERNING EQUATIONS AND TURBULENCE MODEL

For the convenience of modeling, the geometry of the second nozzle is simpler than the practical one, yet it contains the key features of the flow. Normally the second nozzle is made diverged conical shape with four to eight injectors in spinning process. Figure 1 shows a second nozzle

DOI: 10.1002/fld

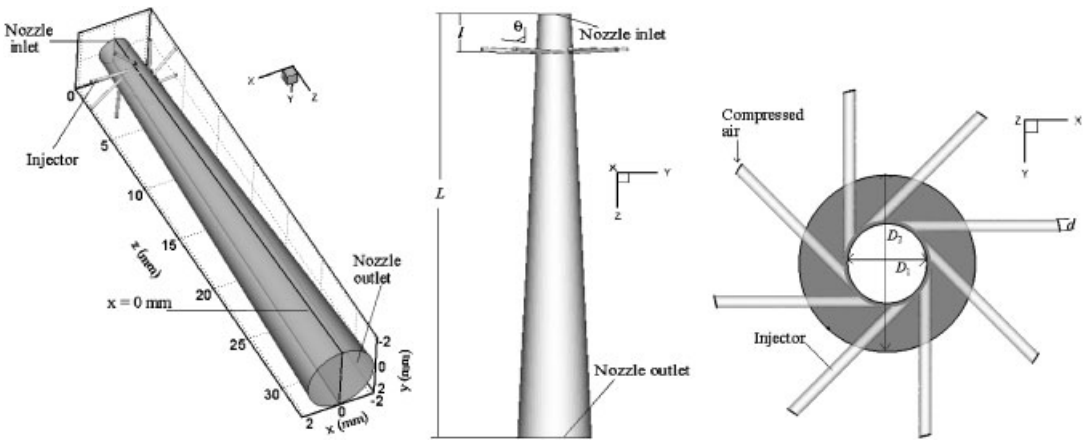

Figure 1. Geometrical profiles of three-dimensional model and projections of the second nozzle.

with eight injectors. In this research, the computational domain is the twisting chamber of the nozzle from the inlet to the outlet, including the injectors. A three-dimensional Cartesian coordinate system as illustrated in Figure 1 is used. The origin of the coordinates system is located at the center of the nozzle inlet. The z-axis is taken as the streamwise direction and the x–y plane is perpendicular to the z-axis (i.e. the nozzle inlet). The diameters of the nozzle inlet D_1 and outlet D_2 are 1.8 and 4 mm, respectively. Also, the nozzle length L is 33 mm, the diameter of the injector d is 0.28 mm and the injection angle θ is 86°. In order to study the effect of the injector position l on the fluid field, it is changed from 3 to 7 mm.

Since high-velocity compressed air is forced into the twisting chamber through the injectors from the air reservoirs, its Mach number is large (on the range of 0.6–0.9) [6, 12], compressibility effects are important. For compressible flows, the modeling of its equations is often made with two kinds of averages: velocity components (u_i), temperature (T) and total energy (e) are Favre mass-weighted averaged while a Reynolds average is used for density (ρ) and pressure (p). Therefore, unsteady, compressible flows the Favre-averaged mean governing equations in Cartesian tensor notation can be written as follows:

$$\frac{\partial \bar{\rho}}{\partial t}+\frac{\partial}{\partial x_i}(\bar{\rho}\tilde{u}_i)=0 \tag{1}$$

$$\frac{\partial}{\partial t}(\bar{\rho}\tilde{u}_i)+\frac{\partial}{\partial x_j}(\bar{\rho}\tilde{u}_i\tilde{u}_j)=-\frac{\partial \bar{p}}{\partial x_i}+\frac{\partial}{\partial x_j}(\tilde{\tau}_{ij}-\overline{\rho u_i'' u_j''}) \tag{2}$$

$$\frac{\partial}{\partial t}(\bar{\rho}\tilde{e})+\frac{\partial}{\partial x_j}(\bar{\rho}\tilde{u}_j\tilde{e})=-\frac{\partial}{\partial x_j}\left[\tilde{u}_j\bar{p}+\tilde{u}_i(\overline{\rho u_i'' u_j''}-\tilde{\tau}_{ij})+C_p\left(\overline{\rho u_j'' T}-\frac{\mu}{\mathrm{Pr}}\frac{\partial \tilde{T}}{\partial x_j}\right)\right] \tag{3}$$

$$\bar{p}=\bar{\rho}(\gamma-1)\left(\tilde{e}-\frac{\tilde{u}_k\tilde{u}_k}{2}-k\right) \tag{4}$$

where an overbar indicates the mean with Reynolds averaging. A tilde and a double prime are corresponding ones for Favre averaging. In addition, μ, k, γ, C_p, Pr and $\tilde{\tau}_{ij}$ are laminar viscosity,

DOI: 10.1002/fld

the turbulence kinetic energy, the ratio of specific heats, specific heat capacity, Prandtl number and the mean viscous stress tensor, respectively.

In the present study, the realizable KEM [30] is adopted to close Favre-averaged equations. Unlike the standard k–ε model, the realizable KEM satisfies certain mathematical constraints on the Reynolds stresses, consistent with the physics of turbulent flows. The modeled transport equations for k and ε in the realizable KEM are:

$$\frac{\partial \bar{\rho} k}{\partial t} + \frac{\partial}{\partial x_i}(\bar{\rho}\tilde{u}_j k) = \frac{\partial}{\partial x_i}\left[\left(\mu + \frac{\mu_t}{\sigma_k}\right)\frac{\partial k}{\partial x_j}\right] + G_k - \bar{\rho}\varepsilon - Y_M \tag{5}$$

and

$$\frac{\partial (\bar{\rho}\varepsilon)}{\partial t} + \frac{\partial}{\partial x_i}(\bar{\rho}\tilde{u}_j \varepsilon) = \frac{\partial}{\partial x_i}\left[\left(\mu + \frac{\mu_t}{\sigma_\varepsilon}\right)\frac{\partial \varepsilon}{\partial x_j}\right] + \bar{\rho} C_1 S\varepsilon - \bar{\rho} C_2 \frac{\varepsilon^2}{k + \sqrt{v\varepsilon}} \tag{6}$$

where $C_1 = \max[0.43, \eta/(\eta+5)]$ and $\eta = Sk/\varepsilon$.

In these equations, S is the mean rate-of-strain tensor, μ_t is a turbulent viscosity, G_k represents the generation of turbulence kinetic energy due to the mean velocity gradients. Y_M is the contribution of the fluctuating dilatation in compressible turbulence to the overall dissipation rate. The constants used in this model are defined: $C_2 = 1.9$, $\sigma_k = 1.0$, $\sigma_\varepsilon = 1.2$.

3. SOLUTION PROCEDURE AND BOUNDARY CONDITIONS

In the present computation, the mean conservation governing equations together with the turbulence model equations are solved numerically by finite-volume scheme based on the FLUENT code. The air was modeled as the ideal gas. Owing to compressible effects, the coupled implicit approach is adopted. It performs a simultaneous solution of the conservation of mass, momentum, energy, turbulent kinetic energy and its dissipation rate equations within the physical domain. The conservation equations are solved using the second-order upwind scheme, and the other (k and ε) equations use the quadratic upstream interpolation of convective kinematics scheme [31], which provides high accuracy for swirling flows. To avoid convergence difficulty, the calculations are done using a reduced pressure ratio at the boundaries, increasing the pressure ratio gradually in order to reach the final desired operating condition. Convergence is judged not only by examining the scaled residual values (i.e. residual is normalized by the respective the largest absolute value of the residual in the first five iterations) for all solution variables, but also by monitoring the average value of mass-flow-rate on $z = 4$ mm surface. The solution convergence is obtained as the average mass-flow-rate value is converged. In addition, the mass fluxes through $z = 12$ mm surface is checked to ensure that the mass is being conserved, i.e. the ratio of the net mass imbalance to the total flux through the system is below 0.8%.

The solutions of the transport equations require specification of boundary conditions on the computational domain. In air-jet spinning, since the outflow of the first nozzle can influence the flow in the second nozzle, the computed result of the first nozzle [10, 11] is used as the boundary condition for the inlet of the second nozzle. At the injector inlet, because the pressure of the air reservoir is known, pressure inlet condition is specified, which define total pressure P_t, static pressure P_s and static temperature T_{in}. The other inlet flow parameters such as Mach number M_{in},

DOI: 10.1002/fld

velocity v_{in}, density ρ_{in}, turbulence kinetic energy k_{in} and turbulence dissipation ε_{in} are calculated at these conditions:

$$M_{in} = \sqrt{2[(P_t/P_s)^{(\gamma-1)/\gamma} - 1]/(\gamma-1)}, \quad v_{in} = M_{in}\sqrt{\gamma R T_{in}}, \quad \rho_{in} = P_s/(RT_{in})$$
$$k_{in} = (0.07 v_{in})^2, \quad \varepsilon_{in} = C_\mu k_{in}^{1.5}/(0.07d) \tag{7}$$

where R and C_μ are gas constant and empirical constant, respectively.

Owing to the pressure inlet and compressible flow, the pressure outlet conditions at the nozzle outlet are specified, i.e. constant static pressure, backflow total temperature, turbulence intensity and hydraulic diameter. As there exists backflow in the outlet, the convergence solution of the pressure outlet is attained more easily than that of the outflow condition. Even if no backflow is expected in the converged solution, setting realistic values in pressure outlet condition will minimize convergence difficulties in the event that backflow does occur during the calculation.

At the wall, no-slip boundary conditions are applied.

4. RESULTS AND DISCUSSION

4.1. Validation of the numerical code and grid independency

Because there are no experimental data fit for swirling flow in a divergent pipe, the computations were first validated for that of in a cylindrical tube against available experimental data (Figure 2), and then simulation in diverging pipe was carried out. It can be observed from figures that the model prediction differs from the experimental results in the quantitative sense. The model predicts lower velocity, a smaller near-wall zone and a larger center zone. Note that the experimental data is based on the Reynolds similarity. Corresponding to the theory analysis [6] and simulation results [12], the equality of Mach numbers for the prototype and the model is paramount because Mach numbers near the injector outlet is close to 1.0. Therefore, a probable reason that causes the difference between simulation and experiment is that the Reynolds similarity is used in the

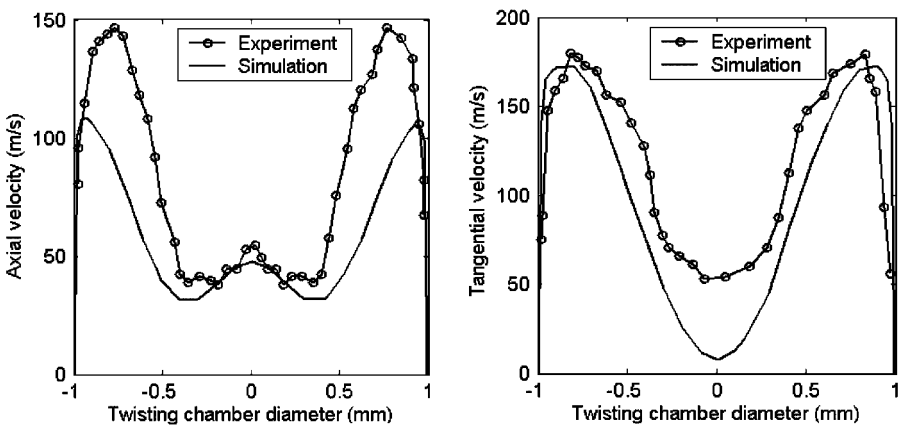

Figure 2. Comparison of the computed axial and tangential velocities profiles with the experimental results of Yu and Zhang [6] in a cylindrical pipe.

DOI: 10.1002/fld

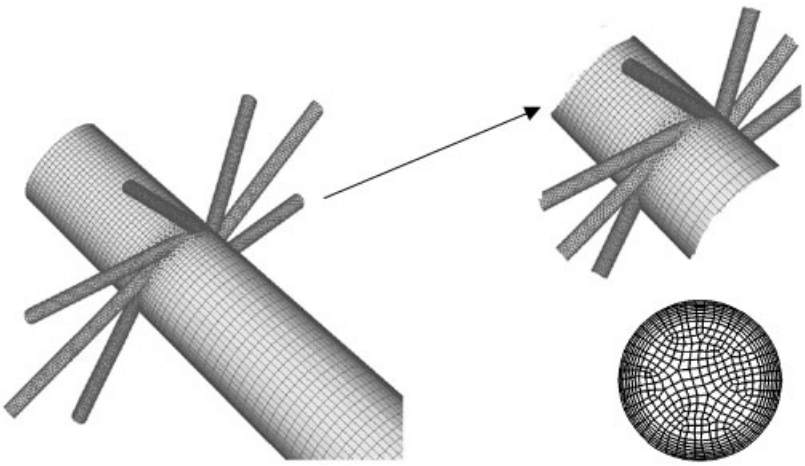

Figure 3. Mesh topology of the nozzle.

measurement. However, in a qualitative sense, the model predicts the velocity distributions quite well, as seen from the figures.

Owing to the sharp-pointed angles, located in the intersection between the injectors and the twisting chamber, a regular mesh is difficult to apply in the entire geometry. A hybrid non-uniform grid is generated (Figure 3). Except the irregular zone including the injectors, the grid discretization in the circumferential direction is uniform, but the radial distribution is chosen in order to increase the number of elementary volumes when getting close to the walls. In the axial direction, a constant discretization is retained, where the cells density is refined as going closer to the irregular part that involves small cells. By this way, a very large difference in cell volume between adjacent cells is avoided. For the irregular zone, we will pre-mesh the edges that represent the intersections between the injectors and the twisting chamber, thereby ensuring a finer mesh in proximity to the sharp-pointed angles Then volume mesh in the irregular zone is created which is composed of triangular and tetrahedral volumes.

Several computational trials were run with various grid resolutions (viz. Grid 1 (152 990), Grid 2 (188 526) and Grid 3 (232 887)) in order to ensure the choice of final grid resolutions. Figure 4 shows the variations of the mean velocity profiles at two axial positions of $z=4$ mm and $z=20$ mm. The results show that the velocities predicted with all the configurations are quite in agreement, except the axial velocities at $z=4$ mm. Therefore, the mesh employed will be deemed to be satisfactory and further refinements of the mesh will not be beneficial. Considering the computational effort, Grid 2 is adopted for all the cases studied.

4.2. General trends analysis of the flow field

A series of time evolution flow structures with the computed streamlines at $x=0$ plane is shown in Figure 5 for the injector position $l=3$ mm. As seen, the swirling flow field experiences a complex flow process before it reaches the steady state. In upstream of injectors, as time is increased, recirculation flow near the wall first is stretched and then is reduced gradually in both the axial and radial directions. In downstream of injectors, the evolution of vortex breakdown is observed. At the

DOI: 10.1002/fld

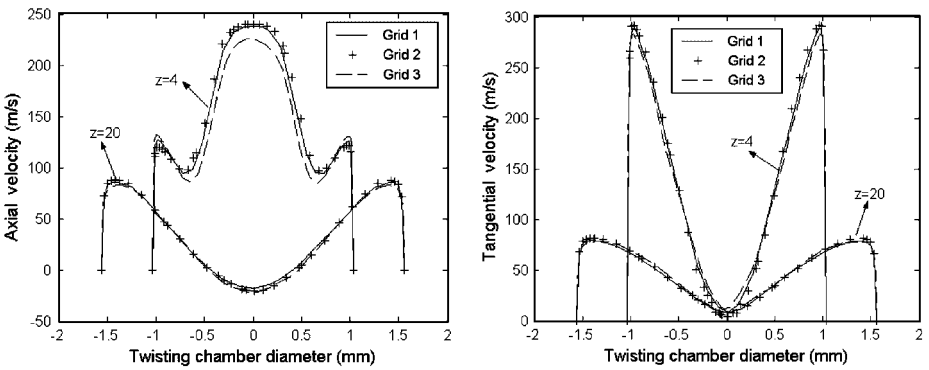

Figure 4. Comparison of mean velocity profiles at different axial locations with various mesh configurations.

initial time step ($t = 5.0 \times 10^{-4}$ s), a central clockwise rotating vortex is formed. Further, the size of the central recirculation vortex is increased as time is increased. As Sarpkaya and Novak [16, 17] pointed out, the conical breakdown could form directly from the closed or axisymmetric bubble breakdown. As seen in Figure 5, the appearance of breakdown is similar to an elliptic bubble type before $t = 1.3 \times 10^{-3}$ s. After that, the breakdown structure is almost nearly axisymmetric with a conical shape. This is also in qualitative agreement with the observations of Brücker [32]. However, internal structure of vortex breakdown is clearly dominated by two asymmetric spiral-like vortices rotating in opposite directions. These spiral-like vortices quickly change shape, followed by another small vortex appearing below the centerline at $t = 1.9 \times 10^{-3}$ s. Then, at $t = 2.0 \times 10^{-3}$ s, just one large vortex is left below the centerline. Note that, at $t = 2.2 \times 10^{-3}$ s, the counterclockwise rotating vortex below the centerline is split again into two small vortices rotating in the same direction. After that, two vortices below the centerline move closer with the upper one growing and the lower one diminishing at $t = 2.4 \times 10^{-3}$ s. Therefore, the flow fluid shows periodic change (see also $t = 2.2$–2.7×10^{-3} s). It is clear from the figures that the stagnation point moves in the downstream direction during this transient period.

The radial distributions of steady-state velocity at different axial locations in the x–z plane are shown in Figure 6. Like tangentially injected swirling flow in a circular pipe [12, 33], the tangential velocity is the largest component, while the radial velocity, whose maximum value is 5% or so of that of the axial velocity, is the weakest of the three velocity components. However, unlike the results in a circular swirl pipe flow [12], the velocity distributions are nearly axisymmetric. This may be because twisting chamber diverges gradually to discharge freely. In addition, the maxima of the three velocity components are located near the wall due to the effect of the centrifugal force, and they decrease gradually with streamwise direction. It is also to be noted, because the injectors are close to the nozzle inlet, that both tangential and axial velocities in upstream of injector are larger than those of slightly further the downstream of the injector.

In Figure 6 the switch from jet-like axial flow upstream of breakdown to wake-like flow downstream of breakdown can be clearly seen. A flow reversal region appears at the center, and its radial extent increases with axial distance to form conical vortex breakdown. However, the magnitude of the reverse flow first increases, and then decreases near the nozzle outlet. The tangential velocity profiles at different axial locations are the same. By identifying the location at which the maximum tangential velocity occurs, the tangential velocity profile can be divided into

DOI: 10.1002/fld

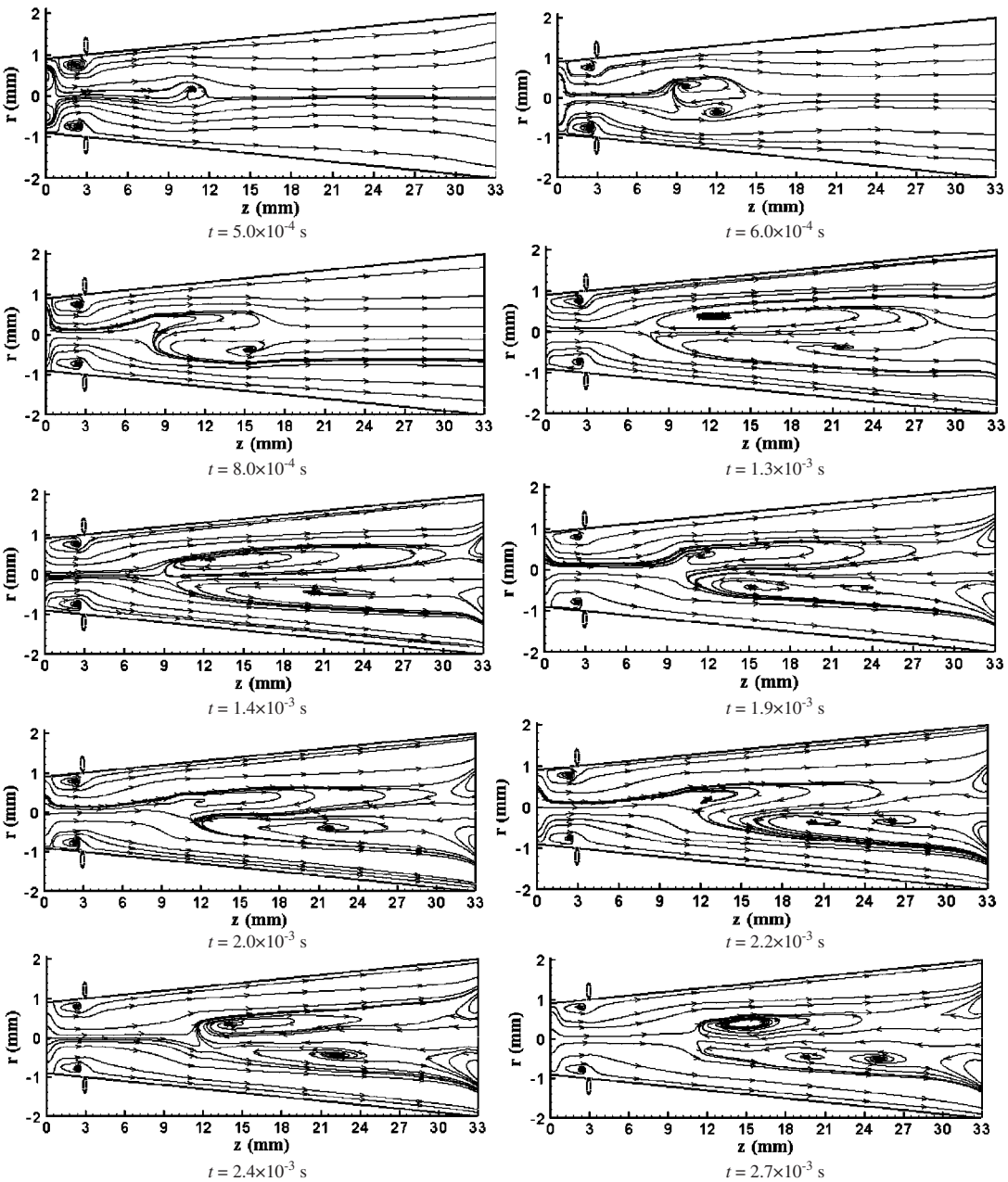

Figure 5. The transient solutions of the streamlines at $x=0$ plane for the injector position $l=3$ mm.

two regions—the core (forced-vortex) and annular (free-vortex) regions. This is in agreement with other works dedicated to swirl motion using incompressible fluid [33]. However, under compressible condition, there is a very small free-vortex zone. According to the velocity distributions, it can be

DOI: 10.1002/fld

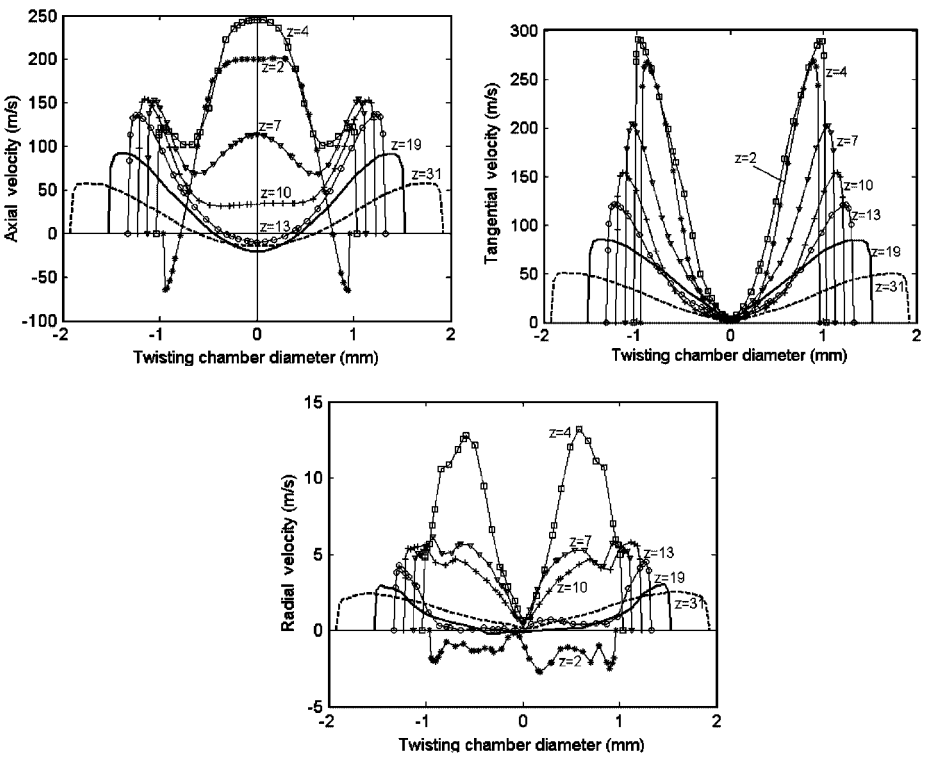

Figure 6. Radial distributions of three steady-state velocity components at different z-axial locations.

inferred that Mach number is the smallest in the center vortex breakdown zone, and it is symmetric. The Mach number approaches 1.0 near the injector outlets. Hence, compressibility effects are important and the flow is subsonic in the twisting chamber.

4.3. The effect of the injector pressure

The injector pressure, which affects the outlet Mach number, is the most important parameter affecting the mechanical properties of air-jet yarns [1–3]. Because the radial velocity is very weak, Figure 7 only shows the axial and tangential velocity profiles along radial direction at different z-axial positions for the different pressures $P = 3.0, 3.5$ and 4.0×10^5 Pa cases. First, for all cases, it is observed that the profiles of velocity distributions are quite similar. Second, as is expected, velocities increase with the increasing injector pressure. However, its increasing trend is not significant, especially far from downstream of the injectors. It is clear from the figures that with pressure increase, both the strength and area of the recirculation near upstream wall do not change significantly. The vortex breakdown location in downstream of the injectors is moved upward with the pressure increase. The simulation results show that the effect of Mach number on the flow field is not significant.

In air-jet spinning, the main function of the second nozzle is to produce uniform steady swirling airflow to untwist the twisting produced by the first nozzle, and make the fiber strand gain true twist.

DOI: 10.1002/fld

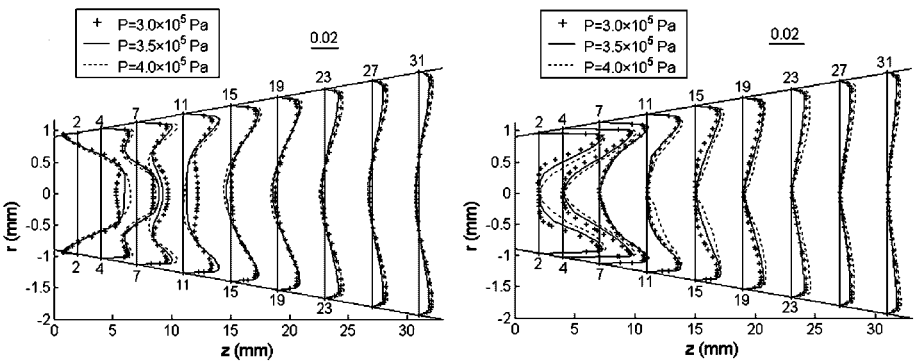

Figure 7. Velocity profiles at different pressures: left figure, axial velocity; and right figure, tangential velocity. The scaling of the shown quantities is given by the number in the upper left corner of the figure.

As the fiber strand passes through the twisting chamber, tangential velocity makes the wrapper fibers impart lateral pressure to the core fiber bundles, and the vortex breakdown helps to form twist difference between edge fibers and the core ones and lead yarn to gain strength by untwisting the false twisted produced by the first nozzle. The simulation results show that the higher injector pressure leads to high spinning tension. This is in agreement with the spinning experimental results by Grosberg *et al.* [1] and Punj *et al.* [34]. From the perspective of energy conservation and the results of the simulation, it is not sensible to increase the injector pressure to a very high level.

4.4. The effect of the injector position

The flow field in tangentially injected swirl flow is strongly dependent on the initial swirl intensity. As indicated by Chang [33], due to conservation of momentum, at the injection location, the local swirl intensity should be equal to the initial momentum flux ratio M_t/M_T, which can be defined as

$$\frac{M_t}{M_T} = \left(\frac{m_t}{m_T}\right)^2 \left(\frac{D}{d}\right)^2 \frac{\sin\theta}{N} \tag{8}$$

where m_t and m_T are the total mass flow rates through the injectors and the test section (i.e. the position at which the compressed air is injected into the twisting chamber), respectively, and D, d, θ and N are the test section diameter, injector diameter, injection angle and injector number, respectively. Owing to changing the cross-sectional area of the twisting chamber, the change of the injector position l will affect the test section diameter D, and further influence initial swirl intensity with other parameters being kept constant. According to Equation (8), as the injectors move downward (i.e. l increases), initial swirl intensity will increase.

Figure 8 depicts several examples of the steady-state particles pathlines for different injection positions. The fluid particles are initially placed on a radial line corresponding to an axial position $z=0$ and three different radii $r=0$, 0.5 and 0.9 mm (for which the nozzle inlet radius is 0.9 mm). For all cases, the pitches of all the pathlines increase gradually with the streamwise direction. Again, the trajectory closest to the wall (at $r=0.9$ mm) forms a large pitch and moves rapidly downstream due to high velocity near the wall (see also Figure 6). It is seen that with the increase in the injection position l, the change of the core spiral's pitch is irregular. A smaller l (=3 mm)

DOI: 10.1002/fld

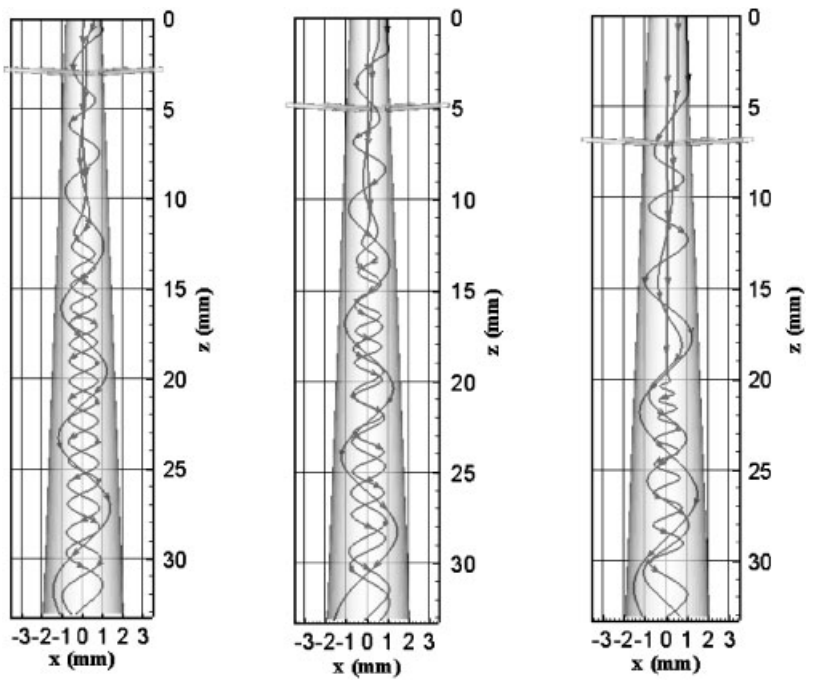

Figure 8. Flow paths of fluid particles for different injection positions, in order from left to right: $l=3$ mm; $l=5$ mm; $l=7$ mm.

will create almost uniform winding and equal pitch in the near axis core region. However, for a larger l (=7 mm), two pathlines starting the radii $r=0$, 0.5 mm will form a large twist difference. Also, along the streamwise direction, the increase in pitch of the central pathline for case $l=7$ mm is the largest compared with that of two other cases. On the other hand, comparison of Figures 5 and 8 shows that the particles trajectories start to become a spiral form when the fluid elements reach recirculation zone. Hence, it can be inferred from Figure 8 that as the injection position l (i.e. initial swirl intensity) increases, the locations of vortex breakdown in downstream of the injectors move downward. This contradicts the results of incompressible fluid in straight pipe by Faler and Leibovich [35] and Chang and Dir [33], who observed that the vortex breakdown migrates upstream toward the inlet with an increase in the swirl intensity. This may be because of both the compressibility effects and the divergence of the pipe. Note that, the recirculation flow in upstream of the injectors is complex, its extent is the largest for $l=5$ mm, while it is the smallest for $l=7$ mm. In accordance with our simulation results and the main function of the second nozzle, a smaller l should be adopted under sufficient suction conditions.

5. CONCLUSIONS

In this work, the turbulent swirling decaying flow induced by means of tangential inlets in a diverged pipe has been numerically investigated using the finite volume package FLUENT. The

DOI: 10.1002/fld

effects of the injector pressure and the injection position on fluid flow are also discussed. Studies of other parameters of the second nozzle will appear in a future publication [36].

As time is increased, the extent of the recirculation zone in upstream of the injectors first increases, and then reduces, while the conical breakdown in downstream of the injector can form from the bubble breakdown. The velocity decays gradually with the axial distance and the maximum values of the three velocity components are located near the wall. The velocities increase with the increasing injector pressure. However, its increasing trend is not significant. The pitches of all the pathlines increase gradually with axial distance, and they tend to increase with the increase in the injection position. In addition, vortex breakdown shifts downstream toward the outlet as the injection position also moves downward.

ACKNOWLEDGEMENTS

This work was supported by the Key Basic Research Foundation of Shanghai under grants No. 08JC1400300.

REFERENCES

1. Grosberg P, Oxenham W, Miao M. The insertion of 'twist' into yarns by means of air-jets, part 1: an experimental study of air-jet spinning. *Journal of the Textile Institute* 1987; **78**(3):189–203.
2. Chasmawala RJ, Hansen SM, Jayaraman S. Structure and properties of air-jet spun yarns. *Textile Research Journal* 1990; **60**(2):61–69.
3. Lawrence CA, Baqui MA. Effects of machine variables on the structure and properties of air-jet fasciated yarns. *Textile Research Journal* 1991; **61**(3):123–130.
4. Heuberger O, Ibrahim SM, Field FC. Technology of fasciated yarns. *Textile Research Journal* 1971; **41**(9):768–773.
5. Tyagi GK, Goyal A. Air-jet spinning: effects on polyester yarns. *The Indian Textile Journal* 2004; **114**(10):17–20.
6. Yu CW, Zhang W. The distribution of airflow field in the nozzle of an air-jet spinning machine. *Journal of China Textile University* 1996; **22**(4):47–57.
7. Zeng YC, Yu CW. Numerical simulation of air flow in the nozzle of an air-jet spinning machine. *Textile Research Journal* 2003; **73**(4):350–356.
8. Gupta AK, Lilley DG, Syred N. *Swirl Flows*. Energy and Engineering Sciences Series. Abacus Press: Tunbridge Wells, U.K., 1984.
9. Guo HF, An XL, Yu CW. Numerical study on the principle of yarn formation in murata air-jet spinning. *Journal of Textile Engineering* 2007; **53**(5):173–178.
10. Guo HF, Chen ZY, Yu CW. Numerical study of an air-jet spinning nozzle with a slotting-tube. *Journal of Physics: Conference Series*, *2007 International Symposium on Nonlinear Dynamics* 2008; **96**:012110-1-5.
11. Guo HF, Chen ZY, Yu CW. Numerical investigation of the function of the slotting-tube in the air-jet spinning. *Journal of the Textile Institute* 2008; 7. DOI: 10.1080/00405000802346321.
12. Guo HF, Chen ZY, Yu CW. 3D numerical simulation of compressible swirl flow induced by means of tangential inlets. *International Journal for Numerical Methods in Fluids* 2008; DOI: 10.1002/fld.1872.
13. Batchelor GK. *An Introduction to Fluid Dynamics*. Cambridge University: Cambridge, England, 1967; 543–555.
14. Buntine JD, Saffman PG. Inviscid swirling flows and vortex breakdown. *Proceedings of the Royal Society of London. Series A*: *Mathematical and Physical Sciences* 1995; **449**:139–153.
15. Rusak Z, Judd KP, Wang S. The effect of small pipe divergence on near critical swirling flows. *Physics of Fluids* 1997; **9**(7):2273–2285.
16. Sarpkaya T. Turbulent vortex breakdown. *Physics of Fluids* 1995; **7**(10):2301–2303.
17. Sarpkaya T, Novak F. Turbulent vortex breakdown experiments. *IUTAM Symposium on Dynamics of Slender Vortices*, Krause E, Gersten K (eds). Kluwer Academic Publishers: Dordrecht, 1998; 287–296.
18. Spall RE, Ashby BM. A numerical study of vortex breakdown in turbulent swirling flows. *Transactions of the ASME Journal of Fluids Engineering* 2000; **122**(1):179–183.
19. Nallasamy M. Turbulence models and their applications to the prediction of internal flows: a review. *Computers and Fluids* 1987; **15**(2):151–194.

20. Khodadadi JM, Vlachos NS. Effect of turbulence model constants on computation of confined swirling flows. *AIAA Journal* 1990; **28**(4):750–752.
21. Chang KC, Chen CS. Development of a hybrid k–ε turbulence model for swirling recirculating flows under moderate to strong swirl intensities. *International Journal for Numerical Methods in Fluids* 1993; **16**(5):421–443.
22. Kim KY, Chung MK. New eddy viscosity model for computation of swirling turbulent flows. *AIAA Journal* 1987; **25**(7):1020–1022.
23. Sloan DG, Smith PJ, Smoot LD. Modeling of swirl in turbulent flow systems. *Progress in Energy and Combustion Science* 1986; **12**(3):163–250.
24. Weber R, Visser BM, Boysan F. Assessment of turbulence modeling for engineering prediction of swirling vortices in the near burner zone. *International Journal of Heat and Fluid Flow* 1990; **11**(3):225–235.
25. Fu S, Huang PG, Launder BE, Leschziner MA. A comparison of algebraic and differential second-moment closures for axisymmetric turbulent shear flows with and without swirl. *Transactions of the ASME Journal of Fluids Engineering* 1988; **110**(2):216–221.
26. Nagendra D. Numerical simulations of an isothermal confined swirling jet in a dump combustor. Retrieved, from the World Wide Web: https://engineering.purdue.edu, 2001.
27. Wang P, Bai XS, Wessman M, Klingmann J. Large eddy simulation and experimental studies of a confined turbulent swirling flow. *Physics of Fluids* 2004; **16**(9):3306–3324.
28. Matsuzaki K, Haramoto Y, Munekata M, Ohba H. A study on swirling flows in a rectangular channel (LDV measurement, flow visualization and large eddy simulation). *Journal of Thermal Science* 2001; **10**(3):205–210.
29. Freitag M, Klein M. Direct numerical simulation of a recirculating swirling flow. *Flow*, *Turbulence and Combustion* 2005; **75**:51–66.
30. Shih TH, Liou WW, Shabbir A, Zhu J. A new k–ε eddy-viscosity model for high Reynolds number turbulent flows. *Computers Fluids* 1995; **24**(3):227–238.
31. Leonard BP. A stable and accurate convective modelling procedure based on quadratic upstream interpolation. *Computer Methods in Applied Mechanics and Engineering* 1979; **19**:59–98.
32. Brücker CH. Some observations of vortex breakdown in a confined flow with solid body rotation. *Flow*, *Turbulence and Combustion* 2002; **69**:63–78.
33. Chang F, Dhir VK. Turbulent flow field in tangentially injected swirl flows in tubes. *International Journal of Heat and Fluid Flow* 1994; **15**(5):346–356.
34. Punj SK, Moitra K. Effect of some machine variables on structure and properties of polyester-viscose air-jet spun yarn. *Indian Journal of Fibre and Textile Research* 1998; **23**:85–93.
35. Faler JH, Leibovich S. Disrupted states of vortex flow and vortex breakdown. *Physics of Fluids* 1977; **20**(9):1385–1400.
36. Guo HF, Chen ZY, Yu CW. Numerical study on the effect of geometric parameters of the second nozzle in air-jet spinning. *Journal of the Textile Institute* 2008; 8. DOI: 10.1080/00405000802624768.